Applied Composite Materials (2021) 28:341–368
https://doi.org/10.1007/s10443-020-09855-x

A Pragmatic Approach for Modelling the Viscoelastic-Viscoplastic Behaviour of Short-Fibre Reinforced Thermoplastics Coupled with Anisotropic Damage

Delphine Notta-Cuvier[1] · Mariem Nciri[1,2] · Franck Lauro[1] · Fahmi Chaari[1] · Bassem Zouari[2] · Yamen Maalej[3]

Received: 18 June 2020 / Accepted: 17 November 2020 / Published online: 29 January 2021

Abstract
In this paper, a previously developed viscoelastic-viscoplastic behaviour model for short-fibre-reinforced thermoplastics (SFRT) is enriched with matrix ductile damage and fibre/matrix interfacial debonding constitutive laws. Aiming at industrial applications, model development takes special care to ensure a relatively easy characterisation of material parameters, as illustrated with case of a short-glass-fibre-reinforced polypropylene. Numerical simulations are done to assess the capability of the model to account for all specificities of SFRT behaviour with a particular attention paid on the coupled influence of strain rate and microstructure configuration on the initiation and development of matrix damage and fibre/matrix debonding.

Keywords Short-fibre reinforced thermoplastics · Anisotropy · Damage mechanisms · Viscoelastic-viscoplastic behaviour

1 Introduction

Short-fibre reinforced thermoplastics (SFRT) are more and more appealing for a wide range of technical applications, in particular because of their high stiffness to density ratio resulting from reinforcement with high-rigidity fibres. In addition, SFRT show easy processability by injection-moulding process and more and more by 3D-printing by fused deposition modelling (FDM). In case of injection moulding, composite parts are generally characterised by complex distributions of fibres orientation in the microstructure which are responsible for anisotropy of composite macroscopic mechanical behaviour [1]. Today, the use of SFRT is progressively extended to engineering applications where parts can

✉ Delphine Notta-Cuvier
delphine.notta@uphf.fr

[1] Polytechnic University Hauts-de-France, LAMIH UMR CNRS 8201, 5913 Valenciennes, France

[2] National Engineering School of Sfax (ENIS), LA2MP, B.P., W3038 Sfax, Tunisia

[3] University of Tunis El Manar, ENIT, MAI (LR11ES19), 1002 Tunis, Tunisia

be subjected to severe loading conditions (i.e. characterised by high strain-rate loadings, such as impacts). Therefore, it becomes crucial to dispose of an accurate behaviour model that takes strain-rate sensitivity together with impact of local microstructure configuration (in terms of fibres orientation in particular) into account. More generally, an accurate modelling must first consider all specificities of thermoplastic matrix behaviour, namely viscoelasticity and non-isochoric and pressure-sensitive viscoplasticity. Then, it has to address load transfer at fibre/matrix interface, which is governed by fibre/matrix adhesion and fibre orientation with respect to macroscopic loading. Finally, different damage mechanisms can affect the behaviour of SFRT. It is generally assumed that fibre breakage remains of low importance during life of injection-moulded SFRT because fibres with length higher than the critical length are generally broken during the injection process. However, SFRT behaviour can be affected by ductile damage of thermoplastic matrix but also by debonding at fibre/matrix interface. It is worth noting that both mechanisms are strongly dependent on composite microstructure organisation and are also inter-dependent. For instance, interfacial debonding leads to stress concentration in matrix material, because fibre load-bearing capacity decreases, that may favor matrix ductile damage.

Present modelling therefore aims at taking all those specificities of SFRT mechanical behaviour into account. In addition, since targeting industrial applications, an aim is that developed model can allow cost-efficient numerical simulations, in particular for high-strain-rate loading. Constitutive equations are therefore implemented using an explicit scheme (Abaqus VUMAT). Finally, it is also important to ensure that the identification of related material parameters can be done by involving a limited number of relatively easy-to-perform experimental tests.

Many works in literature are dedicated to SFRT behaviour modelling and rely on direct finite element (FE) analysis on representative cells of the microstructure [2], mean-field homogenization (MFH) techniques or the asymptotic or mathematical theory of homogenization [3–6]. All those approaches are based on solid thermodynamics foundations. Yet, they require the knowledge of some material parameters which are difficult to identify in practice (transverse properties of fibres, e.g.) and may be very difficult to implement when aiming at taking all specificities of SFRT into account. In addition, their use in an industrial context for numerical simulation of high-strain rate loading is still hindered by their prohibitive computational cost (not developed for explicit scheme of computation, in particular). By contrast, present developments follow an alternative approach dedicated to accurate cost-efficient behaviour prediction under high-strain rate loading [7], as briefly exposed in Section 2.1. Another pragmatic aim was to develop constitutive laws which can be fully characterised with a limited number of experiments (matrix behaviour characterisation and a unique test on composite [8]) and the sole knowledge of fibre axial rigidity. As a counterpart, some assumptions are sometimes necessary, the most important one being to consider that fibres carry load only on their axis direction (i.e. radial and hoop strains are neglected compared to axial strain).

Damage in SFRT has also been the object of many experimental and numerical investigations in the literature [9–13]. It has been extensively reported that damage in such materials occurs at the microscopic level according to different physical degradation mechanisms, in particular matrix microcracks and fibre/matrix interfacial debonding. Based on SEM fractographs of specimens of short-glass-fibre reinforced PA6, Horst and Spoormaker [10] have proposed a damage progression scenario in which damage starts at fibre ends, where local stress concentration is the highest, and propagates along the fibre through progressive fibre/matrix interfacial debonding. Then, matrix microcracks may develop and propagate in a way that depends on matrix level of ductility and fibre local

orientations [9, 10]. Similar scenarios have also been reported by Bernasconi et al. [14], Horst and Spoormaker [10] and Sato et al. [12] using in-situ monotonic tests of short-glass fibre reinforced polyamide-66. Fitoussi et al. [15] have experimentally investigated the damage development in a discontinuous glass-fibre-reinforced ethylene-propylene subjected to high strain-rate loading. They noticed a strain-rate dependency of the damage behaviour in the composite material which was mainly due to the viscous behaviour of the matrix material. Recently, the development of X-ray micro-computed tomography (μCT)-technique has allowed the investigation of damage mechanisms in various composite materials [16, 17] and has pushed forward the quantitative analysis of their kinetics [9, 18].

Some interesting modelling approaches combine micromechanical and continuum damage mechanics (CDM) descriptions. For instance, Nguyen and Khaleel [19] have evaluated the effective and damaged stiffness tensors of composites using self-consistent and Mori-Tanaka schemes, for a reference composite with aligned fibres and for a distribution of fibres over all possible orientations. The evolution of cracks in an elastic matrix material was then modelled in CDM framework. The case of elastoplastic matrix material was similarly treated by Lee and Simunovic [20].

Nouri et al. [21] and Meraghni et al. [22] have presented a phenomenological model for fatigue anisotropic damage in short glass fibre reinforced polyamide. They modelled damage anisotropy by assuming an orthotropic behaviour of the injection moulded composite and using longitudinal, transversal and shear damage state variables. An anisotropic ductile damage of matrix material was also modelled in the framework of continuum damage mechanics by our team [23]. A unique scalar damage variable was introduced but a 4^{th}-order damage tensor was built to take the influence of local fibre orientations into account.

In addition to matrix ductile damage, modelling of the interface degradation in SFRT has received a lot of interest in recent past. One of the proposed models consists in the consideration of an interphase as a third phase of the material [24]. The main drawback in such a three-phase model is that mechanical properties of the interphase are very difficult to identify. A promising way is the development of nanoindentation technique [25] but numerous issues are still to be overcome. In other approaches, Hashin [26, 27] considered the stress and displacement jump at the imperfect fibre/matrix interface to adress damage by fibre/matrix debonding. Despringre et al. [28] used a probabilistic debonding criterion combined to the shear lag model to determine stress state of partially debonded fibres. Our team has modelled fibre/matrix debonding through degradation of load transmission from matrix to fibres [29], as a result of progressive propagation of voids along fibre length, after their initiation at fibre tips (following experimental observations by Sato et al. [12] - cf Section 2.2.2).

Present work is a step forward in the development of a SFRT behaviour model in the continuity of previous developments [7, 8, 23, 29]. As highlighted before, the model is dedicated to behaviour prediction under a wide range of strain rate and aims at taking all specificities of SFRT into account, in particular strain-rate sensitivity, obviously, but also inter-dependent damage phenomena, in direct correlation with microstructure properties. Developments follow a pragmatic approach to reach the best compromise between prediction accuracy and numerical cost efficiency as well as to enable a relatively easy-to-perform experimental characterisation of all involved material parameters. This article is dedicated to the coupling of the different “bricks” of the model, i.e. non damageable viscoelastic (VE)-viscoplastic (VP) constitutive laws for matrix material, matrix ductile damage with anisotropy induced by microstructure heterogeneity and fibre/matrix debonding (Section 2). Identification of damage laws is presented is Section 3 for the case of a short-glass fibre reinforced polypropylene. Finally, a deep analysis of modelling capabilities and limitations

is proposed in Section 4. In particular, coupled influence of fibres complex distribution of orientation and strain-rate on composite behaviour but also on preponderance of one or other damage mechanisms is examined.

2 Constitutive Model

In this section, the modelling of matrix, fibres and composite behaviour is presented. Constitutive laws for virgin materials have been presented in details in previous works [7, 8] and only those which are necessary to introduce damage modelling will be recalled here.

2.1 Modelling of Non-Damageable Behaviour

For modelling purposes, the composite material is seen as the assembly of a matrix medium and several fibre media. Fibres with similar orientation, geometrical characteristics and mechanical properties are grouped into a same medium. In practice, histograms of fibres orientation, length, radius and Young modulus are considered which are divided into n_{ori}, n_L, n_r and n_E intervals, respectively ($n = 1$ if a constant property is considered). Then, the number of fibre media is given by $N_f = n_{ori} \times n_L \times n_r \times n_E$. Finally, a volume fraction is attributed to each fibre medium consistently with the actual distributions of geometry/orientation, that may be characterised by μ-CT, for instance [1, 8], and of Young modulus, possibly (in the present study fibres' Young modulus is assumed to be constant). Behaviour of fibre media and matrix material are successively computed before the composite 3D-stress state is determined based on an additive decomposition of the specific free energy potential [7]. The strain-rate dependent behaviour of matrix material is modelled using a coupled viscoelastic (VE)-viscoplastic (VP) scheme in the framework of small deformation and considering the additive partition of total strain, ε, into a viscoelastic part, ε^{ve}, and a viscoplastic part, ε^{vp} [8]. The Cauchy stress tensor of the matrix material, $\sigma_M(t)$, is linearly related, at an instant t, to the history of VE strain via Boltzmann's hereditary integral:

$$\sigma_M(t) = \int_0^t R^{ve}(t-\zeta) : \frac{\partial \varepsilon^{ve}(\zeta)}{\partial \zeta} d\zeta \tag{1}$$

where R^{ve} is the fourth-order relaxation tensor, expressed using the generalised Maxwell model for linear viscoelasticity [8].

Viscoplasticity is also modelled considering a pressure sensitive and non-isochoric viscoplastic flow. More precisely, viscoplastic flow is predicted considering the Raghava yield surface [30] coupled with a viscous overstress approach in the framework of non-associated viscoplasticity. Note that all kinds of hardening laws can be considered, for instance non-linear exponential laws [8].

Load applied to the matrix material is transferred to embedded fibres through fibre/matrix interface. As already stated, the presence of fibres with different properties and orientations in the composite material is modelled by the coexistence of N_f media. As fibre Poisson ratio and transverse rigidities are very difficult to identify experimentally, a choice was made to assume that all fibres carry load only in their axis direction. So, fibres axial stress is computed using a modified shear-lag model considering an isostrain state with matrix material in fibre axis direction, as described hereafter.

Note that to avoid unphysically lower transverse stresses in the composite than in unreinforced matrix, fibres transverse stresses are then computed assuming an isostress state with a fictitious purely elastic matrix material, which leads to transverse stresses slightly higher than those which would be obtained with Reuss assumption [23].

Fibres axial stress is computed considering that each fibre medium α ($\alpha \in \{1, ..., N_f\}$) behaves unidimensionally with a linear elastic response. Each medium is therefore characterised by its elastic modulus, E_F^α, its orientation vector in global coordinates system, $\mathbf{a}^\alpha$, its geometric properties (i.e. diameter and length) and its volume fraction, v_F^α, so that $\sum_{\alpha=1}^{N_f} v_F^\alpha = v_F = 1 - v_M$. v_F and v_M are respectively the total volume fraction of fibres and matrix in the composite material. As already stated, the computation of fibre axial strain, $\varepsilon_F^{0\alpha}$, is based on the assumption of local iso-strain state between the fibre and the matrix, in fibre axis direction [7]. For each fibre medium α, fibre axial strain is therefore given by $\varepsilon_F^{0\alpha} = A^\alpha \varepsilon A^\alpha$, with A^α the matrix of orientation of fibres in medium α, defined by $A^\alpha = \mathbf{a}^\alpha \otimes \mathbf{a}^\alpha$. Note that A^α is therefore a symetric matrix. A modified shear lag model is then used to compute the average fibre axial stress, $\sigma_F^{0\alpha}$ [7, 31], as follows:

$$\begin{cases} \sigma_F^{0\alpha} = \varepsilon_F^{0\alpha}\left(1 - \frac{E_F^\alpha r^\alpha}{2L^\alpha \tau^\alpha}\left|\varepsilon_F^{0\alpha}\right|\right)E_F^\alpha & \text{if } \left|\varepsilon_F^{0\alpha}\right| \le \frac{L^\alpha \tau^\alpha}{E_F^\alpha r^\alpha} \\ \sigma_F^{0\alpha} = sign\left(\varepsilon_F^{0\alpha}\right)\frac{L^\alpha \tau^\alpha}{2r^\alpha} & otherwise \end{cases} \quad \forall \alpha \in \{1, ..., N_f\} \tag{2}$$

where L^α and r^α are fibre length and radius, respectively, and τ^α is the interfacial shear strength. It is worth re-calling that other components of 3D Cauchy stress tensor of fibres in medium α, σ_F^α, are determined by assuming a quasi iso-stress state between fibres and matrix material in transverse directions with respect to fibre axis [7].

Finally, the composite stress tensor is determined based on the additive decomposition of the composite Helmholtz free energy. The verification of Clausius-Duhem inequality, expressed under the hypothesis of small and isothermal perturbations, for the state potential of the composite material [8] leads to:

$$\sigma_c = v_M \sigma_M + \sum_{\alpha=1}^{N_f} v_F^\alpha A^\alpha \sigma_F^\alpha A^\alpha \tag{3}$$

where σ_c is the 3D Cauchy stress tensor of the composite material.

Those constitutive laws have been validated for the case of a polypropylene reinforced with 30 wt.% short-glass fibres by comparison between numerical simulations (implementation in a VUMAT for Abaqus Explicit) and tensile tests performed at different strain rate (nominal strain rate varying from about 5×10^{-4} to 50 s^{-1}) and different distributions of fibre local orientation with respect to loading direction [8]. The model matched well the experiments for the early stages of loading but, in the vast majority of test cases, predicted composite stress was overestimated from a certain level of strain. This gap was attributed to composite softening resulting from progressive degradation of fibre/matrix interface (i.e. interfacial debonding) and matrix ductile damage, thus demonstrating the necessity to take both phenomena into account in our SFRT behaviour model. Damage laws for thermoplastic matrix and fibre/matrix interface, that take the local properties of microstructure into account, were therefore coupled with SFRT VE-VP behaviour model, as described in the next section.

2.2 Damage Modelling

Damage mechanisms in SFRT highly depend on composite microstructure, particularly on fibres local orientation with respect to macroscopic load direction. As a consequence, matrix damage can become anisotropic in presence of fibres, while being isotropic for unreinforced matrix, due to complex fibres distribution of orientation (cf Section 2.2.1). A 4^{th}-order damage tensor is therefore introduced. Initiation and propagation of fibre/matrix interfacial debonding are governed by fibre axial strain (Section 2.2.2). Therefore, debonding mechanisms are also directly linked to local fibre orientations.

2.2.1 Matrix Damage Law

An anisotropic ductile damage model, based on first developments presented by Notta-Cuvier et al. [23], is coupled here to the matrix VE-VP constitutive laws. Ductile damage of unreinforced thermoplastic matrix is assumed to be isotropic but can become fully anisotropic when matrix is reinforced by short fibres. Indeed, it is assumed that fibres locally prevent matrix damage along their direction of orientation, since fibres bear the major part of loading in that direction. In a given composite volume, characterised by a complex distribution of fibre orientation, matrix damage therefore becomes anisotropic due to cumulated influence of each fibre. Given that fibres with the same orientation are grouped into the same medium, intermediate 4th-order damage tensors, $\mathcal{D}^{\alpha}$, are introduced to link real, $\sigma_M^{0\,\alpha}$, and effective, $\tilde{\sigma}_M^{0\,\alpha}$, matrix Cauchy stress tensors expressed in the coordinates system related to fibre medium α (Eq. 4). More precisely, $\sigma_{M_{11}}^{0\,\alpha} = \tilde{\sigma}_{M_{11}}^{0\,\alpha}$, and $\sigma_{M_{ij}}^{0\,\alpha} = (1-D)\tilde{\sigma}_{M_{ij}}^{0\,\alpha}$ for $i,j \in \{1,2,3\}$ and $(i,j) \neq (1,1)$. These tensors actually stand for stress tensors of a fictitious matrix which would be reinforced by only one medium of aligned fibres. D is the matrix damage scalar state variable, defined in the framework of continuum damage mechanics [32].

$$\sigma_M^{0\,\alpha} = \mathcal{D}^{\alpha}\tilde{\sigma}_M^{0\,\alpha} \;\; i.e. \; \sigma_{M_{ij}}^{0\,\alpha} = \sum_{k,l=1}^{3} \mathcal{D}_{ijkl}^{\alpha}\tilde{\sigma}_{M_{kl}}^{0\,\alpha} \;\; \forall\alpha \tag{4}$$

where $\mathcal{D}^{\alpha}$ is defined as follows (without any summation):

$$\mathcal{D}_{ijkl}^{\alpha} = \delta_{ik}\delta_{jl}\left[1 - D\delta_{ij}\left(1-\delta_{i1}\right) - D\left(1-\delta_{ij}\right)\right] \;\; \forall\alpha \tag{5}$$

where δ_{ij} is the Kronecker symbol defined by $\delta_{ij} = 1$ if $i = j$ and $\delta_{ij} = 0$ if $i \neq j$.

It is also assumed that each fibre medium α governs matrix damage over a volume fraction of the matrix material equal to v_F^{α}/v_M. It is worth noting that this assumption implies that fibre volume fraction does not exceed 33 %. In fact, this value of fibre volume of influence must be seen as an upper bound. As a consequence, matrix damage in fibre axis direction may be underestimated if the volume in which fibres prevent matrix damage is overestimated. Yet, impact on composite macroscopic behaviour would remain low because weight of matrix response (including damage) in composite one is low compared to that of fibres in fibres axis direction. A global 4th-order damage tensor, $\mathcal{D}$ (Eq. 6), that takes contribution of all fibre media into account, is finally introduced to link the real, σ_M, and effective, $\tilde{\sigma}_M$, matrix Cauchy stress tensors (Eq. 7).

$$\mathcal{D}_{ijkl} = \sum_{\alpha=1}^{N_f} \frac{v_F^\alpha}{v_M} \sum_{p,q=1}^{3} T_{ip}^\alpha \left(T^{\alpha^{-1}}\right)_{qj} \left(T^{\alpha^{-1}}\right)_{pk} T_{lq}^\alpha \mathcal{D}_{pqpq}^\alpha + v'_M(1-D)\delta_{ik}\delta_{jl} \tag{6}$$

$$\sigma_M = \mathcal{D}\tilde{\sigma}_M \tag{7}$$

where T^α is the transition matrix from the global coordinates system to that of fibre medium α, $\forall\alpha \in \{1, ..., N_f\}$. v'_M is the volume fraction of the matrix material that is not affected by the presence of fibres and over which matrix therefore damages isotropically [23].

As a novelty compared to previous work [8, 23], matrix damage law is now coupled with VE-VP scheme. The Helmholtz free energy of matrix material is splitted into a viscoelastic (coupled with damage) and a viscoplastic part [32], so that $\phi_M = \phi_M^{ve,D} + \phi_M^{vp}$. According to Lemaitre [33], $\phi_M^{ve,D}$ is defined by:

$$\rho_M \phi_M^{ve,D} = \frac{1}{2} \int_0^t \int_0^t \frac{\partial \varepsilon^{ve}}{\partial \tau}(\tau) : R^{ve,D}(2t-\tau-\xi) : \frac{\partial \varepsilon^{ve}}{\partial \xi}(\xi) d\tau d\xi \tag{8}$$

where ρ_M is the matrix density. $R^{ve,D}$ is the "damaged" matrix 4th-order relaxation tensor and is defined by $R^{ve,D} = \mathcal{D}R^{ve}$.

The evolution of the 4^{th}-order damage tensor, $\mathcal{D}$, is governed by the evolution of the scalar state variable D (Eqs. 5 and 6). D is linked to its conjugate variable, the strain energy density release rate, Y, by the state law [33]:

$$Y = -\rho_M \frac{\partial \phi_M}{\partial D} = -\rho_M \frac{\partial \phi_M^{ve,D}}{\partial D} \tag{9}$$

Given the expression of $\phi_M^{ve,D}$ (Eq. 8), Y is expressed by:

$$Y(t) = -\frac{1}{2} \int_0^t \int_0^t \frac{\partial \varepsilon^{ve}}{\partial \tau}(\tau) : \mathcal{D}' R^{ve}(2t-\tau-\xi) : \frac{\partial \varepsilon^{ve}}{\partial \xi}(\xi) d\tau d\xi \tag{10}$$

where $\mathcal{D}' = \partial\mathcal{D}/\partial D$, so that:

$$\mathcal{D}'_{ijkl} = -v'_M \delta_{ik}\delta_{jl} + \sum_{\alpha=1}^{N_f} \frac{v_F^\alpha}{v_M} \sum_{p,q=1}^{3} T_{ip}^\alpha \left(T^{\alpha^{-1}}\right)_{qj} \left(T^{\alpha^{-1}}\right)_{pk} T_{lq}^\alpha \mathcal{D}_{pqpq}^{\alpha'} \tag{11}$$

where $\mathcal{D}_{ijkl}^{\alpha'} = \delta_{ik}\delta_{jl}\left(\delta_{ij}\delta_{i1} - 1\right), \forall\alpha$. With straightforward manipulations, it finally comes:

$$\mathcal{D}'_{ijkl} = -v'_M \delta_{ik}\delta_{jl} + \sum_{\alpha=1}^{N_f} \frac{v_F^\alpha}{v_M} \sum_{p,q=1}^{3} T_{ip}^\alpha \left(T^{\alpha^{-1}}\right)_{qj} \left(T^{\alpha^{-1}}\right)_{pk} T_{lq}^\alpha \left(\delta_{pq}\delta_{p1} - 1\right) \tag{12}$$

It is worth noting that in case of unreinforced matrix, the expression of Y is simplified since $\mathcal{D}'_{ijkl} = -\delta_{ik}\delta_{jl}$, leading to $\mathcal{D}'R^{ve} = -R^{ve}$ and:

$$Y(t) = \frac{1}{2} \int_0^t \int_0^t \frac{\partial \varepsilon^{ve}}{\partial \tau}(\tau) : R^{ve}(2t-\tau-\xi) : \frac{\partial \varepsilon^{ve}}{\partial \xi}(\xi) d\tau d\xi \tag{13}$$

According to Lemaitre [33], the evolution of the damage state variable, D, is related to that of cumulated viscoplastic strain, $\kappa = \sqrt{2/3\varepsilon^{vp} : \varepsilon^{vp}}$, so that:

$$\begin{cases} \dot{D} = \dot{\kappa}\frac{Y}{S} & if \kappa \geq \kappa_D \\ \dot{D} = 0 & otherwise \end{cases} \tag{14}$$

S and κ_D are respectively the damage modulus and damage threshold which corresponds to the cumulated viscoplastic strain from which damage begins. Identification of those material parameters will be described in Section 3.1.

2.2.2 Debonding Law for Fibre/Matrix Interface

The progressive degradation of fibre/matrix interface is modelled based on experimental observations reported by Sato et al. [12] and previous developments [29]. Interfacial debonding is initiated at the tips of fibres which are oriented closely to loading direction, since they are sites of high stress concentration [12]. It leads to the creation of microvoids which then propagate along fibre length with kinetics that depends in particular of fibre orientation with respect to macroscopic loading, since it governs fibre strain and stress states.

Here, interfacial debonding is modelled as a progressive degradation of load transmission from matrix to fibre at the interface. For a given fibre medium α, debonding is assumed to begin when the fibre axial strain reaches a threshold value, ϵ_{th}, and is responsible for voids creation at fibre tips. Note that composite macroscopic strain at debonding initiation is directly correlated with fibre orientation because it is used to compute fibre axial strain (Section 2.1). Then, voids propagate along fibre side from each fibre tip over a length equal to $L^{D\alpha}$. As a result, load transmission by shear process becomes impossible over a fibre length equal to $\delta^\alpha \leq L^{D\alpha}$. The fibre axial stress, $\sigma_F^{0\alpha}$, is therefore updated by replacing L^α by $L^\alpha - 2\delta^\alpha$ so that:

$$\begin{cases} \sigma_F^{0\alpha} = \varepsilon_F^{0\alpha}\left(1 - \frac{E_F^\alpha r^\alpha}{2(L^\alpha - 2\delta^\alpha)\tau^\alpha}\left|\varepsilon_F^{0\alpha}\right|\right)E_F^\alpha & if \left|\varepsilon_F^{0\alpha}\right| \leq \frac{(L^\alpha - 2\delta^\alpha)\tau^\alpha}{E_F^\alpha r^\alpha} \quad \forall\alpha \\ \sigma_F^{0\alpha} = sign\left(\varepsilon_F^{0\alpha}\right)\frac{(L^\alpha - 2\delta^\alpha)\tau^\alpha}{2r^\alpha} & otherwise \end{cases} \tag{15}$$

δ^α is assumed to increase with fibre axial strain following a purely phenomenological law:

$$\begin{cases} \delta^\alpha = a\left(\frac{\epsilon_F^{0\alpha} - \epsilon_{th}}{\epsilon_{th}}\right)^b \frac{L^\alpha}{2} & if \ \epsilon_F^{0,\alpha} \geq \epsilon_{th} \quad \forall\alpha \\ \delta^\alpha = 0 & otherwise \end{cases} \tag{16}$$

where a and b are constant parameters to be identified.

3 Identification of Damage Laws

The VE-VP-damage model is applied to an injection-moulded polypropylene (PP) reinforced with 30 wt.% of short glass fibres (PP-30GF). Viscoelastic and viscoplastic properties of the PP matrix, short-glass fibres geometrical properties and orientations and interfacial shear strength have already been characterised [8]. In this article, only experiments that are performed to identify the damage laws are therefore presented.

3.1 Identification of Matrix Damage Law

As exposed in Section 2.2.1, damage of matrix material in the composite is strongly influenced by fibre orientations but damage kinetics is driven by a unique scalar damage state variable, D (Eq. 14). Actually, it is likely that matrix damage kinetics is influenced by the presence of fibres, especially because of local modification of plastic flow due to possible areas of stress concentration. Nevertheless, it is experimentally not possible to separate the influence of matrix damage from that of interfacial debonding on SFRT mechanical response to characterise both phenomena from tests on composite. For that pragmatic reason, it is assumed that damage growth in reinforced matrix obeys the same law that in unreinforced matrix, i.e. parameters S and κ_D in Eq. (14) remain the same. Characterisation of matrix damage law can therefore be performed in a easy way by experiments on unreinforced matrix (for which damage is isotropic).

In practice, cyclic loading/unloading tests are performed on PP specimens with a prescribed displacement rate of ± 1 mm.min^{-1} (length of Region Of Interest is 30 mm). All details are given in Appendix. Values of in-plane strain components are computed on specimen's ROI by using Digital Image Correlation technique (VIC2D software). Post-treatment is performed on the area of homogeneous axial strain inside the ROI, which is identified as the central part of the ROI but with a restricted length of about 17 mm. The cyclic stress-strain response is shown in Fig. 1 (last unloading phase is truncated due to loss of correlation).

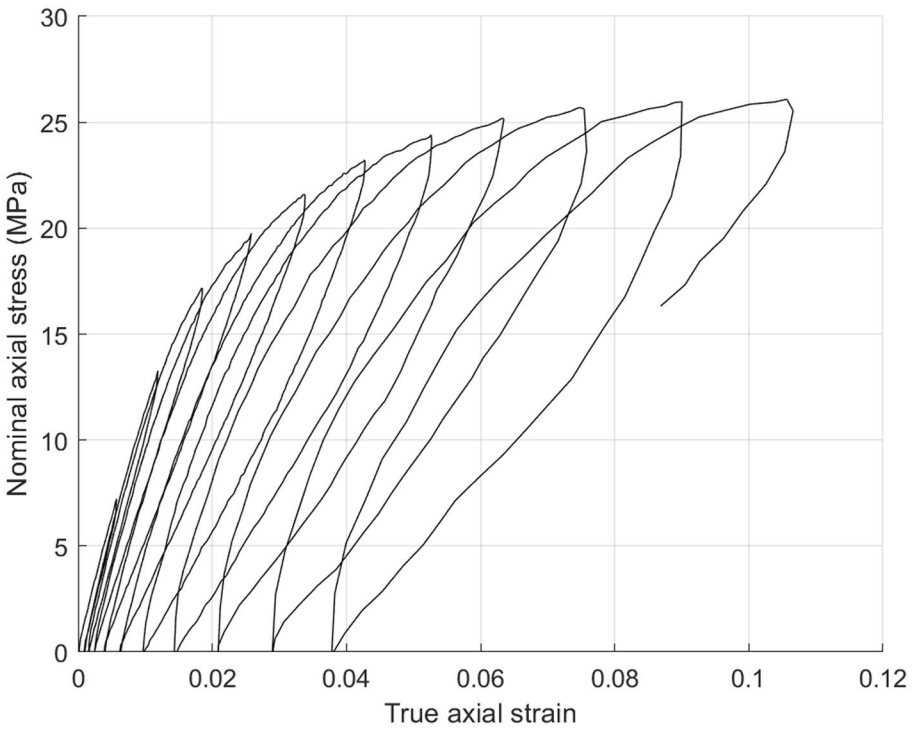

Fig. 1 Cyclic behaviour of unreinforced PP for damage identification

Matrix isotropic damage law (Eq. 14) is identified based on the gradual change of apparent "elastic" modulus, as a non-direct measurement method [20, 34]. Yet, loading and unloading paths are strongly non-linear (Fig. 1), which is attributed to the coupling between viscoelasticiy, viscoplasticity and damage. As a consequence, the "classical" method [33], which consists in linking damage growth to the ratio of apparent and virgin elastic modulus cannot be used directly. As described in Appendix, it is first necessary to separate the contribution of the 3 phenomena in the decrease of apparent moduli. This is done by identifying an evolution law for the effective (i.e. undamaged) modulus during unloading, thus allowing damage computation by comparison between effective and measured apparent moduli for all the cycles. The strain energy release rate, Y, is also computed. As described in Appendix, its computation is greatly simplified since a 1D stress state is considered here. Finally, plotting $\partial D/\partial \kappa$ vs Y allows the identification of parameter S in the damage law (Eq. 14) (see Appendix). A value of 9.23×10^{-2} MPa is thus identified for S and the damage threshold in terms of cumulated viscoplastic strain, κ_D, ranges between 1.9×10^{-3} and 3.3×10^{-3}. From now on, a value of 2.5×10^{-3} will be considered.

3.2 Identification of Debonding Parameters

Identification of debonding parameters in Eq. (16) is performed based on a unique tensile test on SFRT specimen.

Based on SEM in-situ tensile tests, Sato et al. [12] have estimated that debonding initiates at the interface of fibres oriented in loading direction at approximately half of the ultimate load. This observation will be considered here for the estimation of ε_{th}. Growth of debonded length, δ, at fibre/matrix interface then obeys Eq. (16) where parameters a and b must be identified. It is worth recalling that this law of evolution has at the moment no physical fundations. Further works, using nanoindentation at the interface for instance, have to be undertaken in the future to better understand and model debonding mechanisms and kinetics. But, at the moment, an inverse approach is used to fit the proposed law with experimental composite behaviour.

As debonding initiation is favoured at the interface of fibres oriented in tensile loading direction, the specimen which presented the most important proportion of fibres oriented in loading direction, as determined by μ-CT analysis, was selected for the identification of debonding law (Eq. 16), namely specimen PP30-0-10D. Indeed, this choice ensures that weight of debonding in composite tensile response will be maximized, thus leading to a robust characterisation of debonding law. It is worth noting that microstructure of specimen PP30-0-10D was actually not analysed by μ-CT but it was assumed that it is similar to that of a scanned specimen which was cut at the same location in another injected plate (low discrepancy of fibre distributions of orientation from one plate to another was previously verified).

Parameters a and b involved in the evolution of δ^{α} (Eq. 16) have to be identified. From observations on tensile behaviour of PP-30GF [8], it is clear that debonding evolution cannot be linear. The value of exponent b should therefore be greater than 1. Because of coupled influence of a and b on evolution of debonded length, an infinity of couple of parameters can lead to the same debonding law, as illustrated by Fig. 2, and cannot be discriminated in terms of physical meaning. So, the value of b is arbitrarily fixed at 2 while a is identified based on a fit with experimental data, as described below.

For the identification of parameter a, tensile response of specimen PP30-010-D is simulated using a finite element model in ABAQUS Explicit. A user-defined material

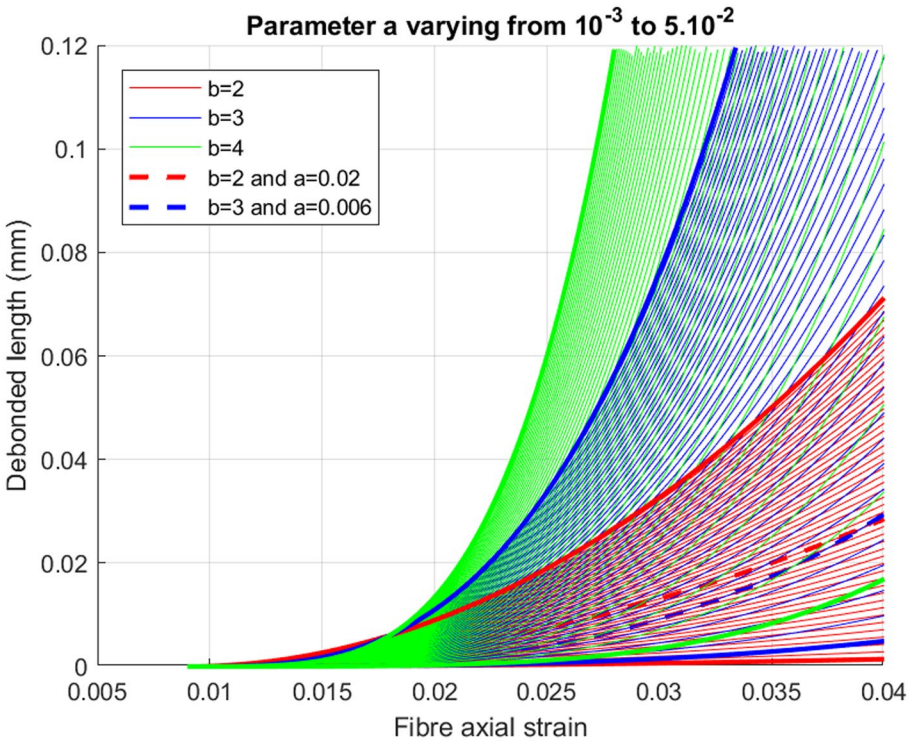

Fig. 2 Influence of parameters a and b on debonded length

(VUMAT) is implemented based on constitutive equations of the VE-VP-damage model. 9 fibre media are considered, with orientations and corresponding volume fractions resulting from a discretization of the actual distribution of fibre orientation (note that those data can be found in Table 1 in Section 4.2). Material parameters of constitutive laws of virgin matrix material are those previously identified [8] and matrix damage parameters are those identified in the previous section. The composite axial strain at 50% of ultimate load is taken as debonding threshold, so that $\varepsilon_{th} = 9 \times 10^{-3}$. Finally, an inverse approach is applied and the value of a is iterated until the best fit between numerical and experimental responses is obtained. A value of $a = 0.02$ is identified.

Figure 3 demonstrates good fit between experimental response and numerical prediction, for example of tensile specimen PP30-0-10D, loaded at a nominal strain rate of $5\,s^{-1}$. In particular, modelling of damage phenomena leads to a good prediction of composite behaviour softening.

4 Discussion

In this section, we assess the capability of the present model to account for specificities of matrix damage and fibre/matrix interfacial debonding in short-fibre reinforced composites. A particular attention is paid on the influence of local fibre orientation and strain rate on unreinforced matrix or composite mechanical response and on the predominance of one or

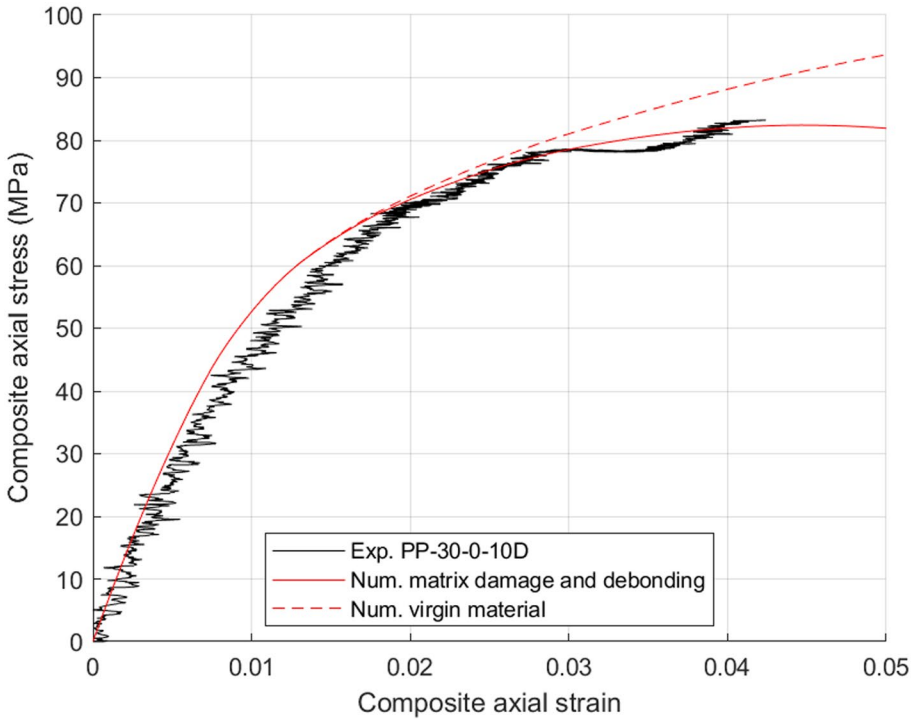

Fig. 3 Numerical prediction of experimental behaviour of PP-30-0-10D specimen (tension 5 s^{-1})

other phenomenon. Numerical simulations are based on a very simple case, namely one cubic element (length of 1mm – C3D8R in Abaqus Explicit). All degrees of freedom of nodes located at the basis of the element (i.e. y=0 here) are blocked. Unless otherwise specified, a uniaxial tensile loading is imposed in the form of velocity loading upon **y**-axis on the upper nodes (i.e. y=1mm here). Material parameters are those identified or reminded in previous sections.

4.1 Modelling of Matrix Damage

Unreinforced matrix A first step consists in analysing the influence of strain rate on evolution of damage in unreinforced polymeric material. Different traction velocities are imposed to reach nominal strain rate of 5, 50 and 500 s^{-1}. Fibre volume fraction is obviously set to 0. Figure 4 shows that the growth of damage variable with respect to matrix axial strain logically goes faster when increasing the strain rate, in accordance with Eq. (14). It can be noted that experiments performed at 5 s^{-1} led to a strain at break for unreinforced PP of about 0.1 (with quite high discrepancy). It would correspond to a critical damage value of about 0.22.

Qualitative comparisons of volume energy of deformation can be done by computing the area under the tensile behaviour curve, σ_{yy} vs ε_{yy}, expressed by:

$$A_{yy} = \int_0^{\varepsilon_{max}} \sigma_{yy} d\varepsilon_{yy} \tag{17}$$

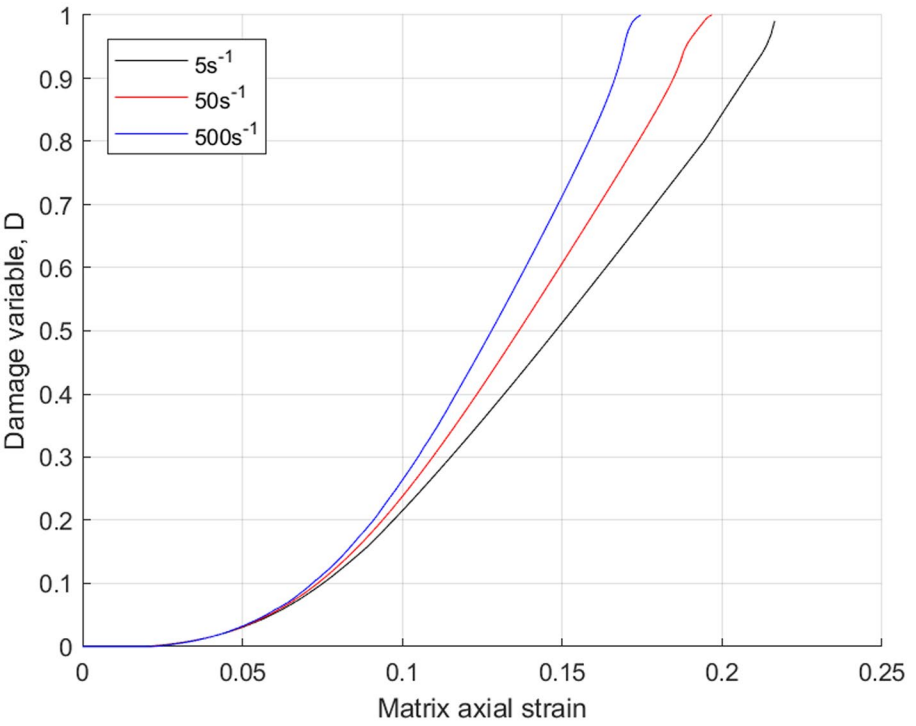

Fig. 4 Damage evolution in unreinforced matrix for different strain rates

where ϵ_{yy} and σ_{yy} are respectively the matrix axial strain and true stress. Figure 5a shows values of A_{yy} up to $\epsilon_{max} = 0.1$. It is clear that the energy of deformation increases with the strain rate, due to viscous effects, but also that the importance of behaviour softening caused by damage increases with strain rate, as confirmed by Fig. 5b. Indeed, relative gap between A_{yy} of damaged vs virgin matrix material increases from about 8% at 5 s^{-1} to about 11% at 500 s^{-1}.

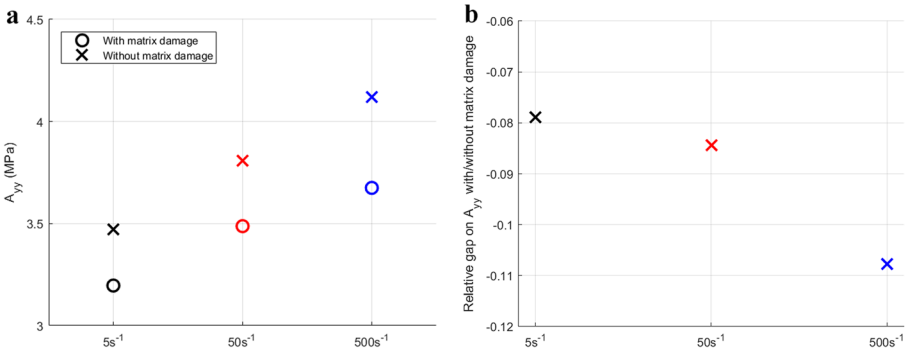

Fig. 5 Influence of damage on area under tensile behaviour curve of unreinforced matrix

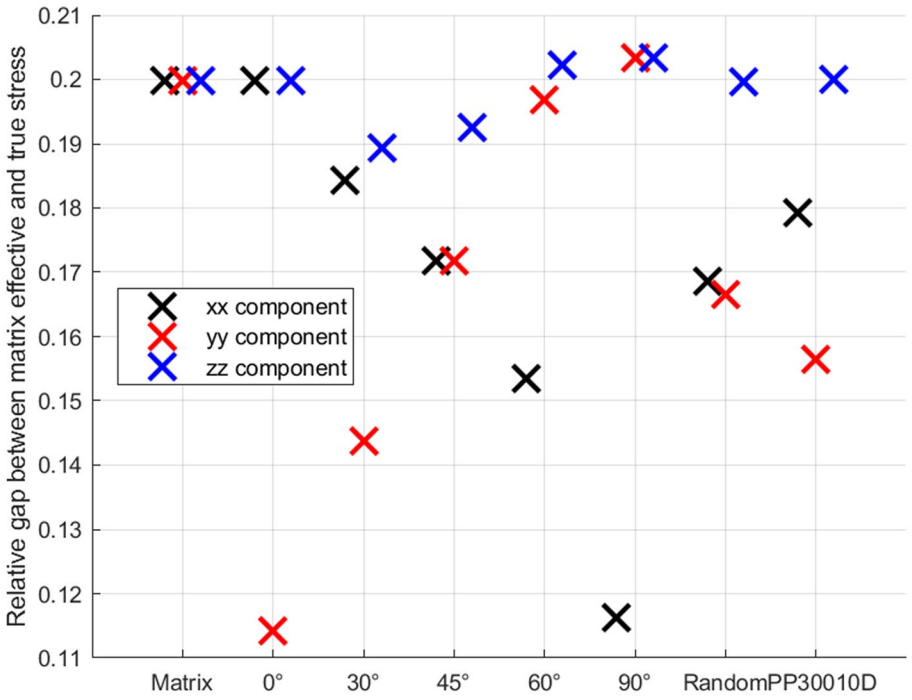

Fig. 6 Anisotropy of matrix damage in presence of short-glass fibres for different fibres orientation

Matrix reinforced by short fibres PP-GF composite material is now considered with fibre volume fraction varying from 10 to 30 %. Different fibre orientations in $(\mathbf{x}, \mathbf{y})$ plane with respect to **y** axis (loading direction) are considered. Interfacial debonding is not taken into account. The impact of matrix damage is first analysed in terms of relative gap between true and effective matrix stress components, i.e. $\frac{\tilde{\sigma}_{Mij}-\sigma_{Mij}}{\tilde{\sigma}_{Mij}}$, at the time step for which the output value of D is the closest to 0.2. As can be seen in Fig. 6 for a fibre content of 30 % and as strain rate of 5 $s-1$, all stress components of unreinforced matrix are affected in the same proportion due to isotropic damage evolution. Yet, matrix damage in composite materials becomes anisotropic. Actually, fibres prevent matrix damage in fibre axial direction. When fibres are all oriented in loading direction (i.e. fibres at 0°), matrix damage is therefore prevented in **y** direction and relative gap between σ_{Myy} and $\tilde{\sigma}_{Myy}$ is lower than for xx and zz components. Note that the gap is not null since the part of matrix material which is not affected by the presence of fibres damages isotropically (cf Section 2.2.1). At the opposite, fibres at 90° prevent matrix damage in **x** direction, which explains why the gap between σ_{Mxx} and $\tilde{\sigma}_{Mxx}$ is this time lower than for other components. Finally, when fibres adopt intermediate orientation, the anisotropy evolves logically, decreasing the gap between σ_{Myy} and $\tilde{\sigma}_{Myy}$ and increasing the gap between σ_{Mxx} and $\tilde{\sigma}_{Mxx}$ when fibre angle of orientation with respect to **y** axis increases. It is verified that the relative gap on through-thickness component (zz) of matrix stress tensor is not affected by the presence of fibres since its value is always equal to $(1 - D)$. The same analysis was done for cases of randomly oriented fibres (9 fibre media - "Random") and for the distribution of orientation

of PP30-0-10-D specimen (main orientation at 0°, 9 fibre media PP30010D). Again, matrix damage is anisotropic: damage in **z** direction is not influenced by the presence of fibres while matrix damage is more or less reduced in **x** and **y** directions, depending on fibre orientations.

Finally, the damage anisotropy level also logically depends on fibre content. For example, where all fibres are oriented along loading direction (i.e. along **y** axis), the damage affecting the *yy* stress component logically decreases when increasing the fibre content while remaining the same for *xx* and *zz* components (Fig. 7 - 5 $s-1$).

Area under tensile behaviour curve, A_{yy} (Eq 17), is computed up to an axial strain equal to 0.1. On this strain range, value of damage variable is always lower than 0.24, 0.28 and 0.31 for all investigated composites at 5, 50 and 500 $s-1$, respectively. Figure 8 shows the relative gap between A_{yy} computed with matrix damage in the composite and A_{yy} computed for the virgin composite material, at a fibre volume content of 30%. Like for unreinforced matrix, it is clear that damage is favoured by an increase of strain rate, accordingly to Eq. (14). As expected, composite softening due to matrix damage is limited when fibres are oriented at 0° with respect to loading direction. Yet, composite softening is always lower than that of unreinforced matrix since a part of matrix material remains unaffected by damage in presence of fibres (in fibre axis direction).

In summary, those simple test cases demonstrate the ability of present matrix damage modelling to take strain-rate influence on damage evolution into account, in unreinforced matrix as well as in composite material. Moreover, the strong link between fibre content

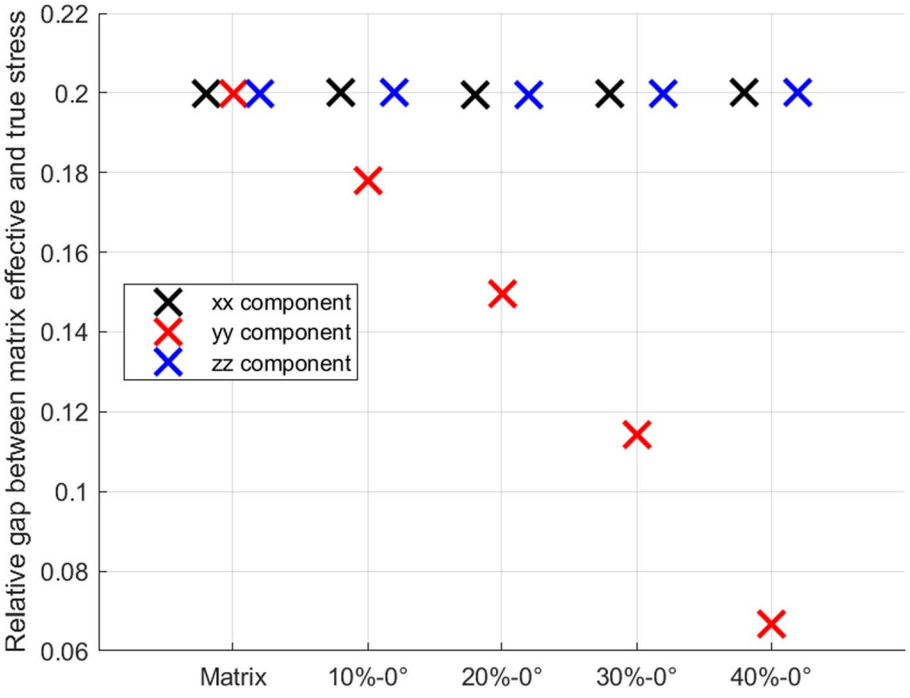

Fig. 7 Anisotropy of matrix damage in presence of different contents of short-glass fibres oriented in loading direction

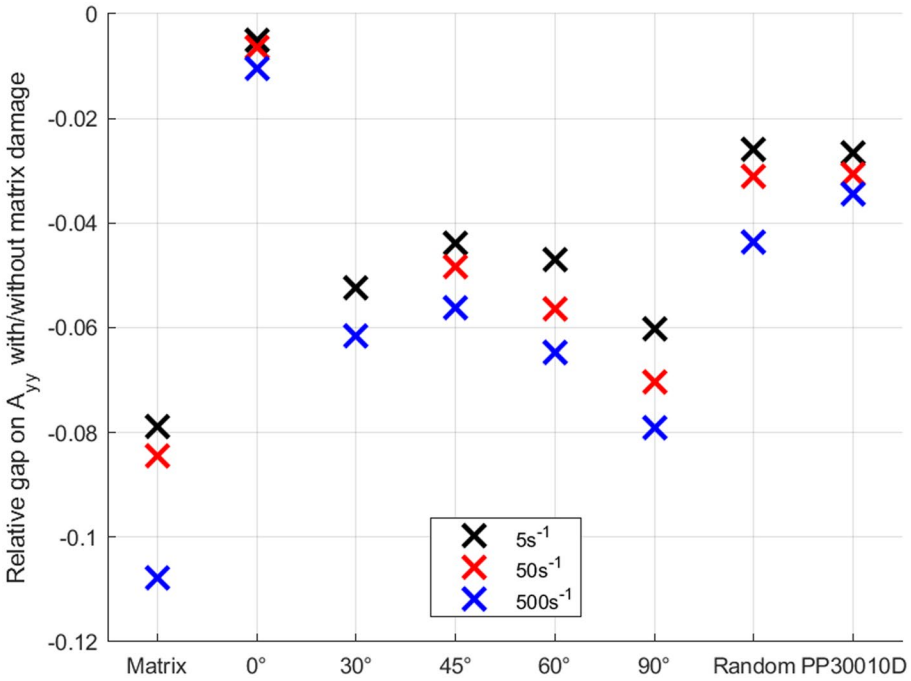

Fig. 8 Influence of matrix damage on composite softening for different fibres orientations

and distribution of orientation, on the one hand, and anisotropy of matrix damage in composite material, in the other hand, is well accounted for.

4.2 Modelling of Interfacial Debonding

The same numerical tests as in previous section are run, for different fibre orientations and strain rate. Matrix damage is not considered but fibre/matrix interfacial debonding is activated as soon as fibre axial strain reaches the previously identified threshold of 9×10^{-3} (see Section 3.2). Actually, for cases with a unique fibre orientation, this threshold is reached only for fibres which are oriented in loading direction, and for fibres oriented at 30° but for unrealistic composite axial strain of 0.32. This observation must be analysed keeping in mind that tests are done on a single cubic element, without blocking of degrees of freedom at the upper nodes. Then, the element deforms in transverse direction and the strain applied to inclined fibres remains quite low. It is not the case when considering several fibre media and debonding is activated at various composite strain level, depending on fibres orientation (Table 1).

So, for present test cases, debonding is activated when all fibres are oriented at 0° but also for random and PP30-0-10D-type orientations. As can be seen on Fig. 9a, debonding leads to a dramatic softening of tensile behaviour of those composites, whereas impact of matrix damage remains low. It is explained by the facts that: 1/ weight of matrix mechanical response in composite behaviour remains lows in presence of fibres oriented in loading direction, therefore the weight of matrix damage remains low too (compared to debonding); 2/ debonded length quickly grows for fibres oriented at 0°, as directly

Table 1 Composite axial strain at initation of interfacial debonding (up to 0.07) in cases of random or distributed fibre orientations

		Random orientation		Distribution of PP30-0-10-D specimen	
Id of fibre medium	Angle vs load direction(°)	Volume fraction	Composite axial strain at debonding initiation (up to 0.07)	Volume fraction	Composite axial strain at debonding initiation (up to 0.07)
1	5	0.0333	0.0105	0.0504	0.0105
2	15	0.0333	0.0140	0.0476	0.0145
3	25	0.0333	0.0214	0.0410	0.0235
4	35	0.0333	0.0382	0.0378	0.0442
5	45	0.0333	Not observed	0.0356	Not observed
6	55	0.0333	Not observed	0.0294	Not observed
7	65	0.0333	Not observed	0.0226	Not observed
8	75	0.0333	Not observed	0.0184	Not observed
9	85	0.0333	Not observed	0.0172	Not observed

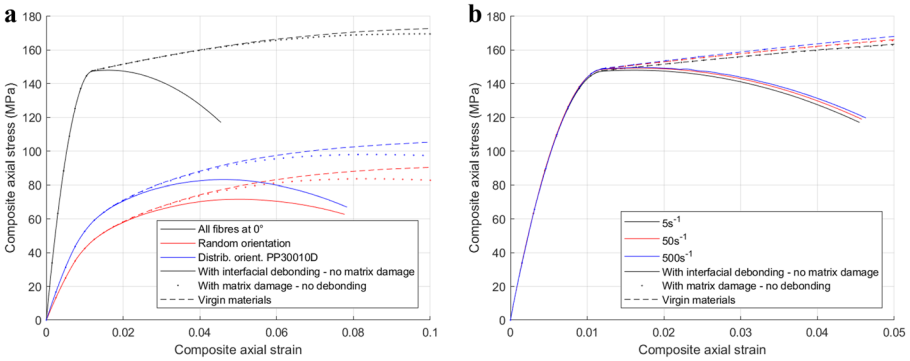

Fig. 9 Influence of interfacial debonding on composite behaviour

increasing with composite axial strain (Eq. 16). Figure 9b shows the low influence of strain rate on composite softening for case of aligned fibres at 0° (same observations for random and PP30010D cases). Indeed, only matrix behaviour is sensitive to strain rate in present modelling, while fibre and fibre/matrix interface (Eq. 16) behaviour are not. Strain-rate sensitivity of composite is therefore only due to matrix viscoelasticity and viscoplasticity. Yet, when the majority of fibres is aligned closely to loading direction, matrix mechanical response represents a minor part of composite behaviour (even if matrix is the majority phase) and then influence of strain rate on composite behaviour remains low.

In summary, activation of interfacial debonding is well modelled, with a composite strain at activation that directly depends on fibres orientation. According to constitutive equations, debonding initiation and propagation is not affected by strain rate. It may constitutes a limitation of present modelling since it would imply that debonding is always the predominant damage mechanism in SFRC, when loading direction is close to fibres principal orientation, whatever the strain rate. Yet, it has often be observed in the literature that, when increasing the strain rate, predominant damage and failure mechanisms can change from debonding to matrix damage. Yet, it is to determined whether it is due to a sensitivity of debonding mechanisms to strain rate or to a drastically decrease of critical void content in matrix at high strain-rate (transition from ductile to brittle damage and failure mechanisms), as often encountered for thermoplastics [34].

In next section, numerical simulations are run with both damage phenomena.

4.3 Association of Both Phenomena

Uniaxial tension As already explained, the weight of matrix damage on composite softening remains low compared to that of debonding, since debonding is only activated when fibres are oriented closely to loading direction (i.e. when composite response is dominated by fibres response). In addition, impact of debonding is rougher than that of matrix damage, as illustrated in Fig. 10. As a consequence, when all fibres are oriented at 0°, the relative gap between area under tensile behaviour curve, A_{yy} (Eq. 17), computed for composite affected only by matrix damage and that computed for virgin material is equal to -9.4×10^{-4} while it increases (in absolute value) up to -4.8×10^{-2} in presence of debonding (composite axial strain up to 0.04). It is to note that the same

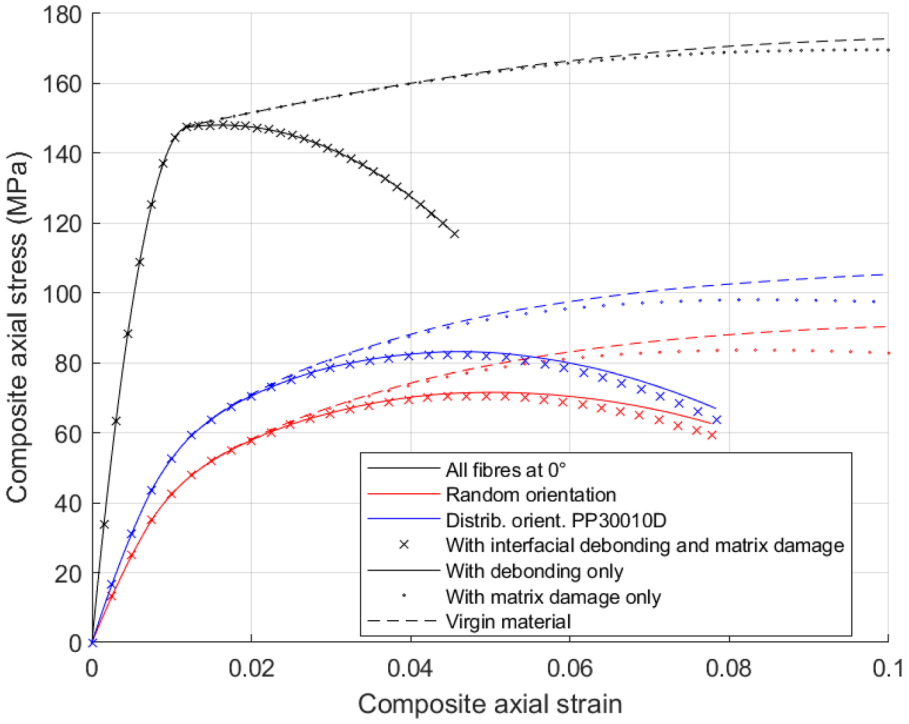

Fig. 10 Influence of both phenomena on composite behaviour

gap is computed with or without matrix damage in presence of debonding, since matrix damage has no impact on composite softening in this range of composite axial strain (Fig. 10 – black curves). When fibres are not all oriented at 0°, for instance for random and PP30-0-10D-type orientations, debonding only affect a reduced proportion of fibres, namely 44.4% and 58.9%, respectively, at a composite strain of 0.07 (Table 1 – composite strain at debonding initiation are the same with or without matrix damage). In addition, debonding does not affect all those fibres from the same composite strain level, but propagates gradually, beginning at interfaces of fibres oriented very closely to loading direction, then affecting interfaces of more oblique fibres (Table 1). So, the impact of debonding on composite softening is less rough and the impact of matrix damage in presence of debonding is, in those cases, visible for moderate composite axial strain (about 0.05 – difference between continuous lines and crosses in Fig. 10). Nevertheless, debonding always remain by far the principal origin of softening of composite response, as illustrated by Fig. 11, where A_{yy} is computed up to a composite axial strain of 0.07.

Finally, as already stated, debonding initiation and evolution is not sensitive to strain rate, contrary to matrix damage. In Fig. 11b, the apparent slight variations between different strain rate are due to some variation of the value of ε_{max} around 0.07, because of slight lag on time of output recording between the simulations.

In summary, for uniaxial tensile loads, debonding is by far the preponderant damage mechanism in SFRC, in presence of fibres oriented close to load direction. The weight of

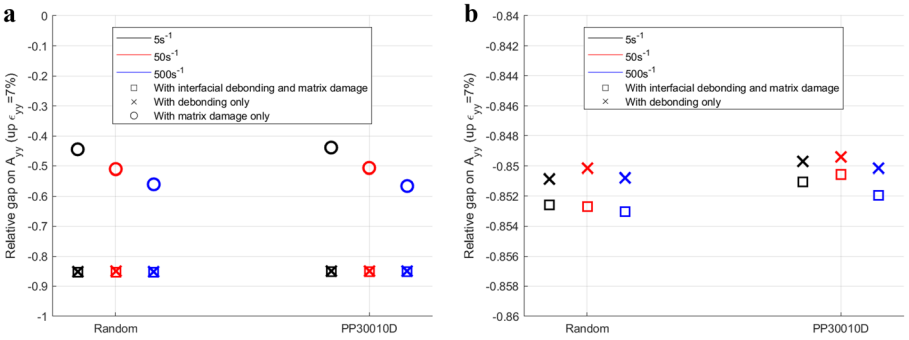

Fig. 11 Composite softening due to both phenomena, for different strain rates

matrix damage in composite softening becomes more important when the proportion of fibres oriented closely to loading direction decreases. Finally, matrix damage becomes the preponderant damage mechanisms when all fibres are oriented with a higher angle with respect to loading direction, simply because fibre axial strain remains too low to lead to an activation of interfacial debonding.

Those observations are valid for simple case of uniaxial tension. In the next paragraph, competition between matrix damage and interfacial debonding is examined for a more complex loading case.

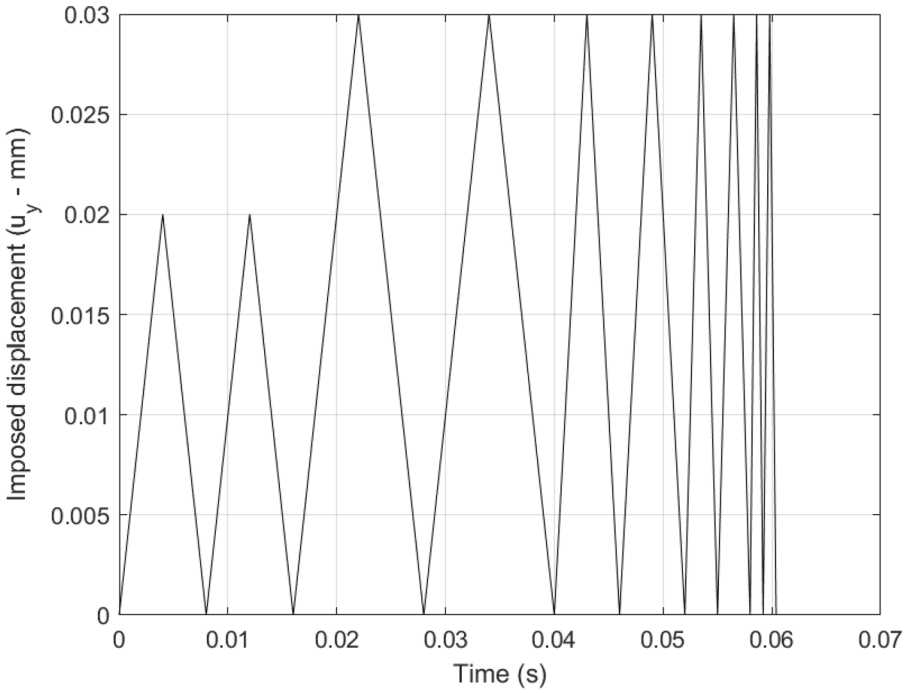

Fig. 12 Cyclic loading

Loading/unloading cyclic test A composite made of matrix material reinforced with 30vol.% glass fibres, all oriented in **y** axis, is subjected to a series of loading/unloading cycles, with imposed displacement along **y** axis (same FE model as before). As shown in Fig. 12, the series starts with two cycles up to u_y=0.02 mm at loading and unloading rate of 5 mm.s^{-1}, followed by cycles up to u_y = 0.03 mm at 5, 10, 20 and 50 mm.s^{-1} (two cycles per loading rate).

This test case has been voluntarily chosen to theoretically favour predominance of debonding vs matrix damage in terms of impact on composite softening. Indeed, considering that fibres are all aligned with loading direction leads to a low weight of matrix response in composite behaviour. In addition, composite axial strain, and therefore matrix axial strain, remains limited to about 0.03, which limits the development of matrix damage (D remains lower than 0.015 - Fig. 13). As a consequence, relative gaps on A_{yy} (Eq. 17) computed during loading phases between composite affected by matrix damage (without debonding) and virgin composite is always lower than 0.34% (in absolute value). In comparison, in presence of debonding relative gaps can reach 10.1%. I

Nevertheless, while remaining limited compared to that of debonding, weight of matrix damage in composite softening is more and more important cycle after cycle, as shown in Fig. 14.

In this Figure, the cumulated relative gaps on A_{yy} after each phase of loading is computed between the composite affected by debonding and matrix damage or debonding only and the virgin composite. It appears that the weight of matrix damage in composite

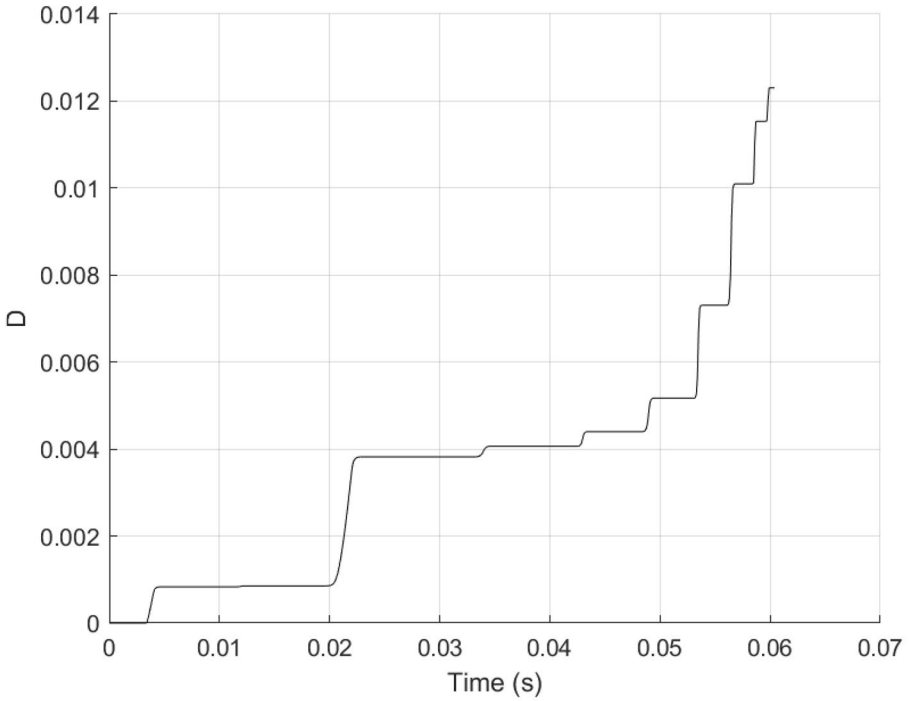

Fig. 13 Growth of matrix damage variable vs time

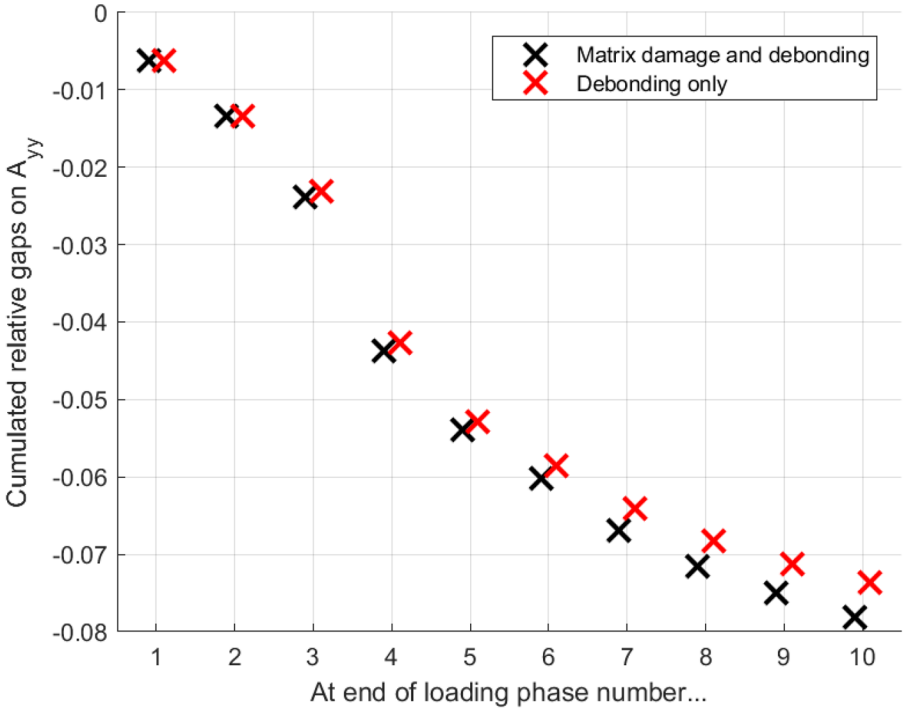

Fig. 14 Increasing influence of matrix damage on composite softening

softening is null or almost for the two first cycles but gradually gains in importance (as illustratred by the increasing gap between black and red crosses).

It is explained by the fact that debonding is iniated at a very early stage of loading (as soon as composite axial strain reaches 0.009 during the first load) and then grows quickly when composite axial strain increases (it is reminded that in that case fibre axial strain is equal to composite axial strain). Yet, after the third cycle, composite axial strain increases

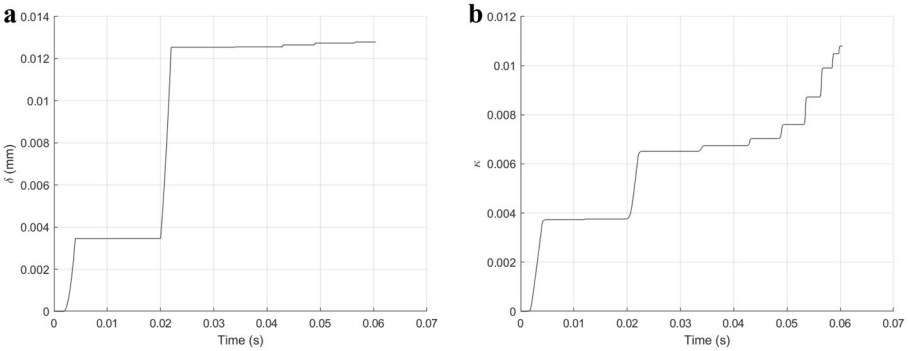

Fig. 15 Evolution of debonded length and cumulated plastic strain vs time

only marginally and so on the debonded length, δ (Fig. 15a). In the same time, the succession of cycles promotes the development of plastic strain in the matrix, as illustrated by the increase of cumulated plastic strain, κ, during each loading phase (Fig. 15b). Therefore, matrix damage keeps on increasing (Fig. 14) while debonding does not evolve anymore.

In summary, present model well reproduces experimental trends for both kinds of damage phenomena, taking influence of strain rate and local fibre orientation into account. Considering the simple case of a composite constituted of aligned fibres in a given direction subjected to uniaxial tension, fibre/matrix interfacial debonding is by far the predominant damage mechanism when fibres are oriented close to load direction. Yet, matrix ductile damage gains in impact as fibre angle increases. In case of complex fibre orientations, the model well reproduces the progressive initiation of debonding, from interfaces of fibres oriented in loading direction at first to interfaces of oblique fibres, as composite axial strain increases. A current limitation of the model remains the absence of interactions between different fibre media for debonding evolution. For instance, it is likely that activation of debonding for fibres oriented at 0° may promote activation of debonding for surrounding fibres, due to possible strain concentration in the matrix. At the contrary, fibres oriented with a high angle with respect to loading direction may act as a barrier for debonding propagation. Finally, when loading favours matrix plastic flow while limiting strain in fibre axis direction (as illustrated here by a series of cyclic loads), matrix damage may develop while interfacial debonding is frozen and can therefore has a non negligible impact on composite softening even in case of fibres oriented in loading direction (i.e. most favourable context for debonding development), while critical debonding length would be reached in uniaxial tension before matrix damage initiation. A limitation of the model may appear here through the absence of interaction between matrix local plasticity state (near the interface) and the promotion/delay of debonding initiation and growth.

5 Conclusion

In this paper, a previously developed viscoelastic-viscoplastic behaviour model for short-fibre-reinforced thermoplastics (SFRT) is enriched with matrix ductile damage and fibre/matrix interfacial debonding constitutive laws.

Matrix damage in the composite can be fully anisotropic depending on local fibre orientations with respect to macroscopic load. A 4^{th}-order matrix damage tensor is therefore built according to microstructure configuration to model fibre influence on reinforced matrix damage. Composite macroscopic behaviour is also affected by debonding at fibre/matrix interface. A phenomenological debonding law that takes local fibre orientation into account is thus introduced.

Characterisation of constitutive laws of both damage phenomena is ensured based on two tests only, if knowing the viscoelastic-viscoplastic behaviour of virgin composite. Indeed, a cyclic loading/unloading test on unreinforced thermoplastic matrix and a uniaxial tensile test on a composite specimen are sufficient to characterise matrix damage and interfacial debonding parameters, respectively.

Numerical simulations on a simple case demonstrate the capability of the model to account for all specificities of SFRT behaviour and in particular the coupled influence of strain rate and microstructure configuration on the initiation and development of matrix damage and fibre/matrix debonding.

In next future, modelling of fibre/matrix debonding have to be improved with more physical-based constitutive laws. Possible paths of research are nanoindentation tests of fibre/matrix interface to better understand and modelling the initiation and kinetics of debonding from the early beginning of void formation. In-situ tensile test in X-ray microtomograph may allow to model the evolution of debonding at a "larger" scale, i.e. when voids growth and propagation become detectable (micrometer scale).

Appendix. Characterisation of Matrix Damage Law

As mentioned in Section 3.1, cyclic loading/unloading tests are performed on PP specimens using an electromagnetic jack (INSTRON E3000) with a 3 kN cell force, at room temperature (20 °C). Specimen geometry follows ISO527 norm, with dimensions of the Region of Interest (ROI) of 5×30 mm^2. Cyclic loadings and unloadings are applied with a prescribed displacement rate of ± 1 mm.min^{-1}. DIC analysis uses a facet size of 15x15 pix^2 (correponding to 0.37x0.37 mm^2) and a subset spacing of 7 pixels, since those parameters led to the best compromise between high signal/noise ratio and spatial resolution. True axial strain is computed as the average of strain measurement in all facets within the homogeneous area of the ROI (length of about 17 mm). It is to note that three tests were realised with very good repeatability.

As mentioned in Section 3.1, it is not possible to directly link the damage growth to the ratio of apparent elastic modulus, $\tilde{E}_c$, and virgin elastic modulus, E, by the relation $\tilde{E}_c = E\left(1 - D_c\right)$ for all loading/unloading cycle c, because of unseparated contributions of viscoelasticity, viscoplasticity and damage on evolution of apparent modulus. A method is therefore proposed here to distinguish damage contribution into modulus evolution in order to identify matrix damage parameters in Eq. (14).

Evolution of Apparent Moduli During Loading/Unloading Cyclic Tests

Unreinforced PP matrix presents strongly non-linear behaviour during loading as well as unloading paths because of viscoelasticity and viscoplasticity. Apparent moduli, potentially affected by damage, $\tilde{E}_{Lc}$ and $\tilde{E}_{Uc}$, are computed during the loading and unloading phase of c^{th} cycle, respectively, with $\tilde{E}_{Lc} = \sigma_{Lc}/(\varepsilon_{Lc} - \varepsilon_{U\,c-1})$ and $\tilde{E}_{Uc} = \sigma_{Lc}/(\varepsilon_{Lc} - \varepsilon_{Uc})$. In previous expressions, σ_{Lc} is the measured true axial stress at the end of c^{th} loading (=beginning of c^{th} unloading), ε_{Lc} and ε_{Uc} are the true axial strain at the end of c^{th} loading and unloading, respectively (for clarity, subscript "yy" indicating loading direction is omitted). Note that the axial stress is null at the end of all unloading phases.

From the first cycle, $\tilde{E}_L$ (during loading) is lower than $\tilde{E}_U$ (during unloading) and both moduli rapidly decreases when the number of cycles increases. Assuming that viscoplastic strain remains constant during unloading, only the apparent modulus upon loading, $\tilde{E}_L$, will decrease due to affectation of tangent modulus during viscoplastic flow. At the

contrary, the strong decrease of $\tilde{E}_U$ cannot be attributed to plastic flow but is the result of viscoelastic strain dissipation and damage. With this hypothesis, the strain partition defined by $\varepsilon = \varepsilon^{ve} + \varepsilon^{vp}$ can be determined at the end of all loading or unloading phases. Thus, at the end of c^{th} unloading phase $\varepsilon^{vp}_{Uc} = \varepsilon^{vp}_{Lc}$ and, if $\varepsilon^{ve}_{Uc} = 0$, then $\varepsilon^{vp}_{Uc} = \varepsilon_{Uc}$. Obviously, $\varepsilon^{ve}_{Lc} = \varepsilon_{Lc} - \varepsilon^{vp}_{Lc}, \forall c$.

Detection of Damage Initiation

Detection of damage initiation is based on the measurement of volume variation during cyclic test, assuming transverse isotropy of the polymer, i.e. equal strain in transverse and thickness direction of the tensile specimen. Theoretically, the transverse strain can be linked to the axial strain using the elastic, ν, and plastic, ν_p, Poisson coefficient. Indeed, $\varepsilon_{xx} = \varepsilon^{ve}_{xx} + \varepsilon^{vp}_{xx} = -\nu\varepsilon^{ve}_{yy} - \nu_p\varepsilon^{vp}_{yy}$. At the end of unloading phases, the total strain is equal to the viscoplastic strain so that $\varepsilon_{xx\,Uc} = -\nu_p\varepsilon_{Uc}\ \forall c$. For the 3 first cycles, this equality is verified for the axial and transverse strains measured by DIC. Yet, from the 4^{th} cycle, the apparent volume variation becomes higher than the theoretical volume variation caused by Poisson effect only, thus indicating that damage has begun. That corresponds to a damage threshold in cumulated vicoplastic strain, κ_D (Eq. 14), which is comprised between 1.9×10^{-3} and 3.3×10^{-3}.

Identification of Viscoelastic Law for Virgin Unloading Apparent Modulus

It is worth noting that the total strain rate is the same (in absolute value) whatever the loading or unloading phases of the test but that the duration of those phases is increasing. A simple viscoelastic Maxwell model is used to model the evolution of virgin (i.e. not affected by damage) apparent modulus, E_U, under uniaxial loading, such that :

$$E_{Uc} = E_\infty + E^{ve} \exp\left(-\Delta^{Uc}t/\tau\right)\ \forall c \tag{18}$$

where $\Delta^{Uc}t$ is the duration of the c^{th} unloading phase.

Parameters E_∞, E^{ve} and τ are identified using a minimisation procedure (genetic algorithm CMAES) with a cost function built from the sum of the square-root gaps between experimental apparent moduli and moduli computed from Eq. (18). Cycles 2 to 4 only are included in the procedure in order to consider virgin apparent moduli. Identified values of E_∞, E^{ve} and τ are respectively of 485 MPa, 1409 MPa and 55.9 s.

Identification of Damage Evolution Law

The identified expression of E_U (Eq. 18) is used to compute apparent virgin moduli for all unloading phases. Value of isotropic damage variable at the end of c^{th} cycle, D_c, is then extracted from the ratio between those virgin moduli and measured moduli, $\tilde{E}_{Uc}$, so that:

$$D_c = 1 - \frac{\tilde{E}_{Uc}}{E_{Uc}} \tag{19}$$

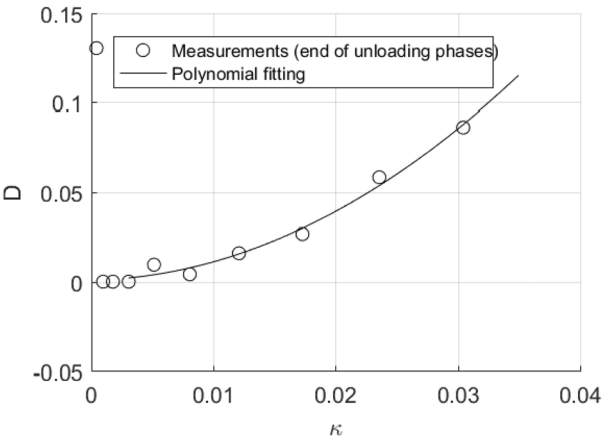

Fig. 16 Evolution of isotropic damage variable vs cumulated plastic strain

Cumulated viscoplastic strain at the end of c^{th} cycle, κ^c, is computed from DIC measurement of in-plane strains, considering that the viscoplastic part of the total strain is equal to the residual strain at the end of each unloading phase, i.e. $\kappa_c = \sqrt{2/3}\sqrt{\left(\varepsilon_{xx\,Uc}\right)^2 + \left(\varepsilon_{yy\,Uc}\right)^2 + 2\left(\varepsilon_{xy\,Uc}\right)^2}$. Evolution of D vs κ is given in Fig. 16.

Following Lemaitre [33] theory, the strain energy release rate, Y, can be expressed from the viscoelastic energy of deformation, ω_e, so that:

$$Y = \frac{\omega_e}{1-D} = \frac{\frac{1}{2}\int \sigma_{ij} d\varepsilon_{ij}^{ve}}{1-D} \tag{20}$$

where ε^{ve} and σ are respectively the viscoelastic strain tensor and the true Cauchy stress tensor.

In present case of uniaxial stress state along y axis, the expression of ω_e is greatly simplified and $\omega_e = 1/2\,\sigma_{yy}\varepsilon_{yy}^{ve}$. In addition, $\tilde{\sigma}_{yy} = \sigma_{yy}/(1-D)$ and $\tilde{\sigma}_{yy} = E_U\varepsilon_{yy}^{ve}$ at the end of loading phases. Finally, it comes a simplified expression for Y at the end of the c^{th} loading phase:

$$Y_c = \frac{\sigma_{Lc}}{2\left(1-D_c\right)}\frac{\tilde{\sigma}_{Lc}}{E_{Uc}} \Rightarrow Y_c = \frac{\sigma_{Lc}^2}{2E_{Uc}\left(1-D_c\right)^2} \tag{21}$$

Then, damage parameter, S (Eq. 14), is identified by linear regression on the curve of $\partial D/\partial\kappa$ vs Y (which slope is equal to $1/S$), plotted with values computed at the end of all loading phases. To this aim, a second-order polynomial fitting is done to express the evolution of D vs κ, which leads to $D^{fit} = 89.67\kappa^2 + 0.1336\kappa + 8.61\,10^{-4}$ (continuous line in Fig. 16). Then, value of $(\partial D/\partial\kappa)_c$ is approximated by $\left[D^{fit}\left(\kappa_c + \delta\kappa\right) - D^{fit}\left(\kappa_c - \delta\kappa\right)\right]/2\delta\kappa$, with $\delta\kappa = 10^{-4}$. Linear regression between $\partial D/\partial\kappa$ vs Y (Fig. 17) leads to a slope value of 10.84 MPa^{-1}, i.e. S=9.23×10^{-2} MPa.

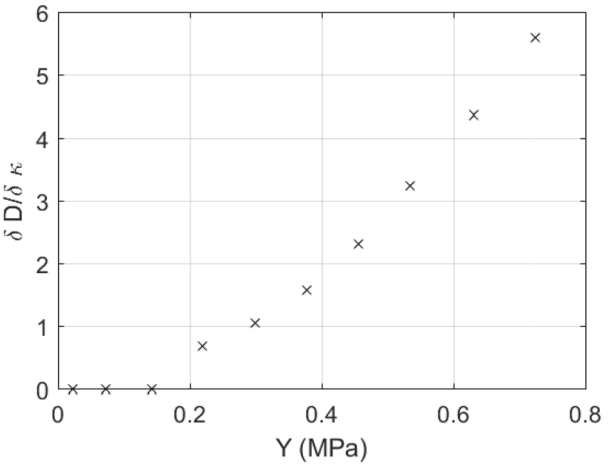

Fig. 17 Identification of damage parameter S: $\partial D/\partial \kappa$ vs Y

Acknowledgements The authors sincerely thank Dr. Remi Delille, Dr. Gregory Haugou and Dr. Fréderic Robache (University Polytechnic Hauts-de-France) for their precious assistance during experimental tests. The authors gratefully acknowledge the support of CISIT Program, Hauts-de-France Region, French Minister of Higher Education and Research, National Center for Scientific Research and the European Community. Dr Nciri acknowledge the support received during her phD through the collaboration between the University Polytechnic Hauts-de-France and the National Engineering School of Sfax in the frame of the Utique CMCU programme.

References

1. Notta-Cuvier, D., Nciri, M., Lauro, F., Delille, R., Chaari, F., Robache, F., Haugou, G., Maalej, Y.: Coupled influence of strain rate and heterogeneous fibre orientation on the mechanical behaviour of short-glass-fibre reinforced polypropylene. Mech. Mater. **100**, 186–197 (2016)
2. Charles III, L.T., Liang, E.: Stiffness prediction for unidirectional short-fiber composites: Review and evaluation. Compos. Sci. Technol. **59**, 655–671 (1999)
3. Ghosh, S., Lee, K., Moorthy, S.: Two scale analysis of heterogeneous elastic-plastic materials with asymptotic homogenization and Voronoi cell finite element model. Comput. Methods Appl. Mech. Engrg. **132**, 63–116 (1996)
4. Hill, R.: A self-consistent mechanics of composite materials. J. Mech. Phys. Solids. **13**, 89–101 (1965)
5. Mori, T., Tanaka, K.: Average stress in matrix and average elastic energy of materials with misfitting inclusions. Acta Metallica **21**, 571–574 (1973)
6. Smit, R.J.M., Brekelmans, W.A.M., Meijer, H.E.H.: Prediction of the mechanical behavior of nonlinear heterogeneous systems by multi-level element modeling. Comput. Methods Appl. Mech. Engrg. **155**, 181–192 (1998)
7. Notta-Cuvier, D., Lauro, F., Bennani, B., Balieu, R.: An efficient modelling of inelastic composites with misaligned short fibres. Int. J. Solids and Struct. **50**, 2857–2871 (2013)
8. Nciri, M., Notta-Cuvier, D., Lauro, F., Chaari, F., Maalej, Y., Zouari, B.: Modelling and characterisation of dynamic behaviour of short-fibre-reinforced composites. Compos. Struct. **160**, 516–528 (2017)
9. Arif, M., Saintier, N., Meraghni, F., Fitoussi, J., Chemisky, Y., Robert, G.: Multiscale fatigue damage characterization in short glass fiber reinforced polyamide-66. Composites Part B **61**, 55–65 (2014)
10. Horst, J.J., Spoormaker, J.L.: Fatigue fracture mechanisms and fractography of short-glass fibre-reinforced polyamide 6. J. Mater. Sci. **32**, 3641–3651 (1997)
11. Praud, F., Chatzigeorgiou, G., Bikard, J., Meraghni, F.: Phenomenological multi-mechanisms constitutive modelling for thermoplastic polymers, implicit implementation and experimental validation. Mech. Mater. **114**, 9–29 (2017)

12. Sato, N., Kurauchi, T., Sato, S., Kamigaito, O.: Microfailure behaviour of randomly dispersed short fibre reinforced thermoplastic composites obtained by direct SEM observation. J Mater Sci **26**, 3891–3898 (1991)
13. Schemmann, M., Gorthofer, J., Seelig, T., Hrymak, A., Bohlke, T.: Anisotropic meanfield modeling of debonding and matrix damage in SMC composites. Compos. Sci. Technol. **161**, 143–158 (2018)
14. Bernasconi, A., Davoli, P., Basile, A., Filippi, A.: Effect of fibre orientation on the fatigue behaviour of a short glass fibre reinforced polyamide-6. Int. J. Fatigue **29**, 199–208 (2007)
15. Fitoussi, J., Bocquet, M., Meraghni F.: Effect of the matrix behavior on the damage of ethylene-propylene glass fiber reinforced composite subjected to high strain rate tension. Composites: Part B. **45**, 1181–1191 (2012)
16. Bayraktar, E., Antolonovich, S., Bathias, C.: Multiscale study of fatigue behaviour of composite materials by X-rays computed tomography. Int. J. Fatigue **28**, 1322–1333 (2006)
17. Withers, P.J., Preuss, M.: Fatigue and damage in structural materials studied by X-ray tomography. Annu Rev Mater Res **42**, 81–103 (2012)
18. Cosmi, F., Bernasconi, A.: Micro-ct investigation on fatigue damage evolution in short fibre reinforced polymers. Compos. Sci. Technol. **79**, 70–76 (2013)
19. Nguyen, B.N., Khaleel, M.A.: A mechanistic approach to damage in short-fiber composites based on micromechanical and continuum damage mechanics descriptions. Compos. Sci. Technol. **64**, 607–617 (2004)
20. Lee H.K., Simunovic S.: Modeling of progressive damage in aligned and randomly oriented discontinuous fiber polymer matrix composites. Composites: Part B. **31**, 77–86 (2000)
21. Nouri, H., Meraghni, F., Lory, P.: Fatigue damage model for injection-molded short glass fibre reinforced thermoplastics. Int. J. Fatigue **45**, 934–942 (2009)
22. Meraghni, F., Nouri, H., Bourgeois, N., Czarnota, C., Lory, P.: Parameters identification of fatigue damage model for short glass fiber reinforced polyamide (PA6-GF30) using digital image correlation. Procedia Engineering **10**, 2110–2116 (2011)
23. Notta-Cuvier, D., Lauro, F., Bennani, B., Balieu, R.: Damage of short-fibre reinforced materials with anisotropy induced by complex fibres orientations. Mech. Mater. **68**, 193–206 (2014)
24. Christensen, R., Lo, K.: Solutions for effective shear properties in three phase sphere and cylinder models. J. Mech. Phys. Solids **27**, 315–330 (1979)
25. Hardiman, M., Vaughan, T.J., McCarthy, C.T.: A review of key developments and pertinent issues in nanoindentation testing of fibre reinforced plastic microstructures. Comp. Struc. **180**, 782–798 (2017)
26. Hashin, Z.: Thermoelastic properties of fiber composites with imperfect interface. Mech. Mater. **8**, 333–348 (1990)
27. Hashin, Z.: Thin interphase/imperfect interface in elasticity with application to coated fiber composites. J. Mech. Phys. Solids **50**, 2509–2537 (2002)
28. Despringre, N., Chemisky, Y., Bonnay, K., Meraghni, F.: Micromechanical modeling of damage and load transfer in particulate composites with partially debonded interface. Compos. Struct. **155**, 77–88 (2016)
29. Notta-Cuvier, D., Lauro, F., Bennani, B.: Modelling of progressive fibre/matrix debonding in short-fibre reinforced composites up to failure. Int. J. Solids and Struct. **66**, 140–150 (2015)
30. Raghava, R., Caddell, R.M., Yeh, G.S.Y.: The macroscopic yield behaviour of polymers. J. Mater. Sci. **8**, 225–232 (1973)
31. Bowyer, W.H., Bader, M.G.: On the reinforcement of thermoplastics by imperfectly aligned discontinuous fibres. J. Mater. Sci. **7**, 1315–1321 (1972)
32. Lemaitre, J., Chaboche, J.L.: Mechanics of Solid Materials. Cambridge University Press, England (1996)
33. Lemaitre, J.: A course on damage mechanics. Springer, Berlin Heidelberg (1992)
34. Balieu, R., Lauro, F., Bennani, B., Haugou, G., Chaari, F., Matsumoto, T., Mottola, E.: Damage at high strain rates in semi-crystalline polymers. Int. J. Impact Eng. **76**, 1–8 (2015)